Available online at www.sciencedirect.com
SCIENCE DIRECT®
International Journal of Thermal Sciences 45 (2006) 752–759
International Journal of Thermal Sciences
www.elsevier.com/locate/ijts

Natural convection in a horizontal layer of a binary mixture

M. Ouriemi, P. Vasseur *, A. Bahloul, L. Robillard

Ecole Polytechnique, CP 6079, Succ "Centre Ville", Montréal, PQ H3C 3A7, Canada

Received 25 January 2005; received in revised form 7 November 2005; accepted 21 November 2005

Available online 14 February 2006

Abstract

This paper reports an analytical and numerical study of the natural convection in a horizontal shallow cavity filled with a binary fluid. Neumann boundary conditions for temperature and solute concentration are applied to the two vertical walls of the enclosure. The governing parameters of the problem are the thermal Rayleigh number Ra_T, the aspect ratio A, the buoyancy ratio φ, the Lewis number Le and parameter a. Both double diffusive convection ($a = 0$) and Soret induced convection ($a = 1$) are considered. An analytical model, based on the parallel flow approximation, is proposed for the case of a shallow layer ($A \gg 1$). The particular case where the buoyancy forces induced by the thermal and solutal effects are opposing each other and of equal intensity ($\varphi = -1$) is considered. For this situation the critical Rayleigh number for the onset of supercritical and subcritical convection is predicted. The study is completed by a numerical solution of the full governing equations.

Keywords: Natural convection; Double diffusion; Soret effect

1. Introduction

The growing research of convection in binary mixtures, generated by buoyancy due to simultaneous temperature and concentration gradients, results from its importance in wide range of situations. In nature such flows are encountered in the oceans, lakes, solar ponds, shallow coastal waters and the atmosphere. In industry examples include chemical processes, crystal growth, energy storage, material processing such as solidification, food processing ... etc.

Most studies on this topic are concerned with double diffusive convection in a vertical cavity for which the flows induced by the buoyancy forces result from the imposition of both thermal and solutal boundary conditions on the vertical walls. This flow configuration was first studied numerically and analytically by Trevisan and Bejan [1] for the case of a vertical slot subject to constant horizontal gradients of temperature and concentration. However, as discussed by Alavyoon [2] their solution is good only for the special case of a Lewis number equal to unity and as such does not deal with double-diffusive convection. Ranganathan and Viskanta [3] presented an analytical and numerical study of natural convection in a square cavity filled with a binary gas due to combined temperature and concentration gradients. The existence of multi cell flow structures, for particular values of the Lewis number and the buoyancy ratio, has been demonstrated both experimentally (Han and Kuchn [4] and Lee et al. [5]) and numerically (Lee and Hyun [6] and Shyy and Chen [7]). More recently the problem originally considered by Trevisan and Bejan [1] was re-examined by Mamou et al. [8]. An analytical solution was proposed by these authors in the limit of tall enclosures. This solution was demonstrated to be in good agreement with the numerical solution of the complete governing equations.

A few studies are also concerned with convection, within a vertical cavity, induced by Soret effects. For this situation the species gradients result from the imposition of a temperature gradient in an otherwise uniform-concentration mixture. The first study on this topic is due to Bergman and Srinivasan [9]. Their numerical results indicate that the Soret-induced buoyancy effects are more important when convection is relatively weak. The particular case of a square cavity under the influence of thermal and solutal buoyancy forces, which are opposing and of equal intensity, has been investigated by Traore and Mojtabi [10]. The Soret effect on the flow structures was investigated numerically. The same problem was considered by

* Corresponding author.
E-mail address: patrick.vasseur@polymtl.ca (P. Vasseur).
URL: http://www.meca.polymtl.ca/convection.

1290-0729/$ – see front matter
doi:10.1016/j.ijthermalsci.2005.11.004

Nomenclature

A	aspect ratio of the enclosure, L'/H'
C_S	dimensionless concentration gradient in x-direction
C_T	dimensionless temperature gradient in x-direction
D	mass diffusivity of species
D'	thermodiffusion coefficient
g	gravitational acceleration ..... $\mathrm{m\,s^{-2}}$
H'	height of enclosure ..... m
j'	solute flux per unit area ..... $\mathrm{kg\,m^{-2}\,s^{-1}}$
k	thermal conductivity ..... $\mathrm{W\,m^{-1}\,K^{-1}}$
L'	width of the enclosure ..... m
Le	Lewis number, α/D
S	dimensionless concentration
N	mass fraction
Nu	Nusselt number
Pr	Prandtl number, ν/α
q'	constant heat flux per unit area ..... $\mathrm{W\,m^{-2}}$
Ra_T	Rayleigh number, $g\beta'_T\Delta T' H'^3/\alpha\nu$
Ra_{TC}^{sub}	subcritical Rayleigh number, Eq. (30)
Ra_{TC}^{sup}	supercritical Rayleigh number, Eq. (28)
S	reduced concentration, $N/\Delta N$
Sh	Sherwood number
t	dimensionless time, $t'\alpha/H'^2$
T	dimensionless temperature, $(T' - T'_O)/\Delta T'$
$\Delta T'$	characteristic temperature, $q'H'/k$
u	dimensionless velocity in x-direction, $u'H'/\alpha$
v	dimensionless velocity in y-direction, $v'H'/\alpha$
x	dimensionless coordinate axis, x'/H'
y	dimensionless coordinate axis, y'/H'

Greek symbols

α	thermal diffusivity ..... $\mathrm{m^2\,s^{-1}}$
μ	dynamic viscosity of fluid ..... $\mathrm{kg\,m^{-1}\,s^{-1}}$
ν	kinematic viscosity of fluid ..... $\mathrm{m^2\,s^{-1}}$
ω	vorticity
θ	dimensionless temperature field
φ	buoyancy ratio
ρ	density of fluid ..... $\mathrm{kg\,m^{-3}}$
$(\rho C)_f$	heat capacity of fluid ..... $\mathrm{W\,s\,m^{-3}\,K^{-1}}$
Ψ	dimensionless stream function, Ψ'/α
Ψ_0	dimensionless relation linked to stream function

Subscript

O	reference state

Superscript

$'$	refers to dimensional variable

Krishnan [11] and Gobin and Bennacer [12] for the case of an infinite vertical fluid layer. The critical Rayleigh number for the onset of motion was determined by these authors.

The present investigation is concerned with the case of a shallow layer of a binary fluid submitted to the influence of thermal and concentration horizontal gradients. The solutal buoyancy forces are assumed to be induced either by the imposition of constant fluxes of mass on the vertical walls (double diffusive convection) or by temperature gradients (Soret effects). This problem, despite its practical application, does not seem to have been considered in the literature.

2. Problem statement

The configuration considered in this study is a horizontal shallow cavity, of thickness H' and width L' filled with a binary mixture (see Fig. 1). The origin of the coordinate system is located at the centre of the cavity with x' and y' being the horizontal and vertical coordinates, respectively. All the boundaries are impermeable. Neumann boundary conditions are applied, for both temperature and concentration, on the vertical walls of the layer. The binary fluid is assumed to satisfy the Boussinesq approximation. The density variation with temperature and concentration is described by the state equation $\rho = \rho_O[1 - \beta'_T(T' - T'_O) - \beta_N(N - N_O)]$ where ρ_O is the fluid mixture density at temperature $T' = T'_O$ and mass fraction $N = N_O$ and β'_T and β_N are the thermal and concentration expansion coefficients, respectively.

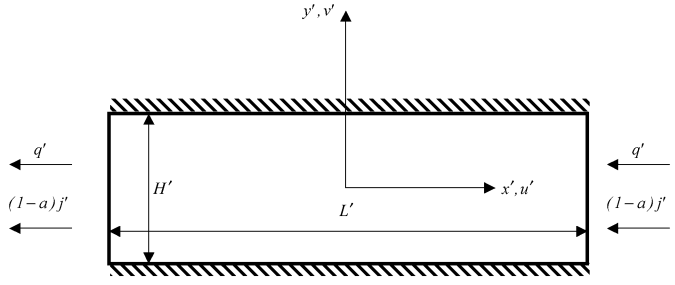

Fig. 1. Schematic diagram of the problem domain and coordinate system.

The phenomenological equations, relating the fluxes of heat $\vec{Q}'$ and matter $\vec{J}'$ to the thermal and solute gradients, present in a binary fluid mixture are given by (see for instance, De Groot and Mazur [13]):

$$\vec{Q}' = -k\nabla T', \qquad \vec{J}' = -\rho D\nabla N - \rho D' N(1-N)\nabla T' \tag{1}$$

where k and D are the thermal conductivity and the isothermal diffusion coefficient. D' is the coefficient for the Soret effect.

The balanced equations for momentum, energy and mass fraction of the denser components are given below in terms of the vorticity ω', stream function Ψ' and velocity field $\vec{V}'$ as:

$$\frac{\partial\omega'}{\partial t'} + J(\Psi', \omega') = \nu\nabla^2\omega' - \frac{g\beta'_T}{\nu}\frac{\partial}{\partial x'}\left(T' + \frac{\beta_N}{\beta'_T}N\right) \tag{2}$$

$$\frac{\partial T'}{\partial t'} + J(\Psi', T') = \alpha\nabla^2 T' \tag{3}$$

$$\frac{\partial N}{\partial t'} + J(\Psi', N) = D\nabla^2 N + aD' N_0(1-N_0)\nabla^2 T' \tag{4}$$

where a is a real number, the significance of which will be discussed in the following text, $\omega' = -\nabla^2\Psi'$, $J(f,g) = f_y g_x - f_x g_y$. As usual, we have: $u' = \partial\Psi'/\partial y'$, $v' = -\partial\Psi'/\partial x'$ such that the mass conservation is satisfied.

In the above equations, ν is the kinematic viscosity of the mixture and α the thermal diffusivity coefficient.

The boundaries conditions applied on the wall of the layer are:

$$x' = \pm\frac{L'}{2}, \qquad \Psi' = \frac{\partial\Psi'}{\partial x'} = 0$$

$$\frac{\partial T'}{\partial x'} = \frac{q'}{k}, \qquad \frac{\partial N}{\partial x'} = \frac{j'(1-a)}{\rho D} - a\frac{D}{D'}N(1-N)\frac{\partial T'}{\partial x'} \tag{5}$$

$$y' = \pm\frac{H'}{2}, \qquad \Psi' = \frac{\partial\Psi'}{\partial y'} = 0, \qquad \frac{\partial T'}{\partial x'} = \frac{\partial N}{\partial x'} = 0 \tag{6}$$

The governing equations are nondimensionalized by scaling the length with H', the stream function with the thermal diffusivity α and the time with α/H'^2. Also, we introduce the reduced temperature $T = (T' - T'_O)/\Delta T'$ and the reduced concentration $S = N/\Delta N$ where $\Delta T' = q'H'/k$ and $\Delta N = -j'/\rho D$ for double diffusive convection ($a = 0$) and $\Delta N = N_O(1-N_O)\Delta T' D'/D$ for Soret-driven convection ($a = 1$). In the above expressions q' and j' are the uniform fluxes of heat and mass per unit area respectively, applied on the vertical walls of the system.

The dimensionless equations governing the present problem then read

$$\frac{\partial\nabla^2\Psi}{\partial t} + J\big(\Psi, \nabla^2\Psi\big) = Pr\,\nabla^4\Psi - Ra_T Pr\frac{\partial}{\partial x}(T + \varphi S) \tag{7}$$

$$\frac{\partial T}{\partial t} + J(\Psi, T) = \nabla^2 T \tag{8}$$

$$\frac{\partial S}{\partial t} + J(\Psi, S) = \frac{1}{Le}\big(\nabla^2 S - a\nabla^2 T\big) \tag{9}$$

The corresponding boundary conditions are

$$x = \pm A/2, \qquad \Psi = \frac{\partial\Psi}{\partial x} = 0$$

$$\frac{\partial T}{\partial x} = 1, \qquad \frac{\partial S}{\partial x} = (1-a) + a\frac{\partial T}{\partial x} \tag{10}$$

$$y = \pm 1/2, \qquad \Psi = \frac{\partial\Psi}{\partial y} = 0, \qquad \frac{\partial T}{\partial y} = \frac{\partial S}{\partial y} = 0 \tag{11}$$

where the case $a = 0$ corresponds to double-diffusive convection for which the solutal buoyancy forces in the liquid layer are induced by the imposition of a constant heat flux q' such that $\partial T/\partial x = 1$ on the vertical boundaries. According to Eq. (10) the corresponding solutal boundary conditions are given by $\partial S/\partial x = 1$. On the other hand $a = 1$ corresponds to the case of a binary fluid subject to the Soret effect.

From the above equations it is observed that the present problem is governed by the thermal Rayleigh number $Ra_T = g\beta'_T\Delta T' H'^3/\alpha\nu$, buoyancy ratio $\varphi = \beta_N\Delta N/\beta'_T\Delta T'$, Lewis number $Le = \alpha/D$, Prandtl number $Pr = \nu/\alpha$, aspect ratio $A = L'/H'$ and parameter a, where g is the gravitational acceleration.

3. Numerical solution

The solution of the governing equations and boundary conditions, Eqs. (7)–(11), is obtained using a control volume approach and the SIMPLER algorithm (Patankar [14]). A finite difference procedure with variable grid size is considered for better consideration of boundary conditions. The power-law scheme is used to evaluate the flow, heat and mass fluxes across each of the control volume boundaries. A second order backwards finite difference scheme is employed to discretize the temporal terms appearing in the governing equations. The discretized momentum, energy and concentration equations are under-relaxed to accelerate the convergence. The relaxation parameter was chosen equal to 0.5. A Thomas iterative procedure is employed to solve the resulting discretized equations. At each new time step, the updating of the physical new variables is done until the convergence criterion $\sum_{i=1}^{m}(b_i^k - b_i^{k-1})/\sum_{i=1}^{m} b_i^k \leqslant 10^{-9}$ is satisfied, where b stands for Ψ, T and S.

Numerical tests have been performed to determine the minimum aspect ratio above which the flow can be assumed to be parallel. In the range of the parameters considered in this investigation it was found that the numerical results can be considered independent of the aspect ratio when $A \geqslant 6$. For this reason most of the numerical results reported here were obtained for $A = 8$ with typically 60×180 mesh points.

The numerical results presented in this study were obtained for the particular case $Pr = 7$. However, the results are not limited to this specific value since it is well known (see for instance Ref. [1]) that the solution is rather insensitive to the Prandtl number provided that this latter is of order one or greater.

4. Analytical solution

In the limit of a shallow cavity $A \gg 1$, the governing equations (7)–(9) can be considerably simplified under the parallel flow approximation $\Psi(x,y) \approx \Psi(y)$, $T(x,y) \approx C_T x + \theta_T(y)$ and $S(x,y) \approx C_S x + \theta_S(y)$, where C_T and C_S are unknown constant temperature and concentration gradients respectively in x-direction (see for instance Ref. [15]).

Using the above approximations, Eqs. (7)–(9) reduce to the following systems of equations

$$\frac{\mathrm{d}^4\Psi}{\mathrm{d}y^4} = Ra_T(C_T + \varphi C_S) \tag{12}$$

$$\frac{\mathrm{d}\Psi}{\mathrm{d}y}C_T = \frac{\mathrm{d}^2\theta_T}{\mathrm{d}y^2} \tag{13}$$

$$\frac{\mathrm{d}\Psi}{\mathrm{d}y}C_S = \frac{1}{Le}\left[\frac{\mathrm{d}^2\theta_S}{\mathrm{d}y^2} - a\frac{\mathrm{d}^2\theta_T}{\mathrm{d}y^2}\right] \tag{14}$$

The contribution of the return flow from the end regions is taken into account via a global balance (Ref. [16]). Making use of the boundary conditions, Eqs. (10), it is found that

$$C_T = \frac{1}{1+I_1} \quad \text{where } I_1 = \int_{-1/2}^{1/2}\Psi^2\mathrm{d}y \tag{15}$$

Similarly, for the mass fraction, it is found that

$$C_S = \frac{(1-a)}{1+Le^2 I_1} + a\frac{(1-Le\,I_1)}{(1+Le^2 I_1)(1+I_1)} \tag{16}$$

The solution of Eqs. (12)–(14), satisfying the boundary conditions (11), is:

$$\Psi(y) = \Psi_O\left[16y^4 - 8y^2 + 1\right] \tag{17}$$

$$\theta_T(y) = \Psi_O C_T\left[\frac{16y^5}{5} - \frac{8y^3}{3} + y\right] \tag{18}$$

$$\theta_S(y) = \Psi_O \alpha\left[\frac{16y^5}{5} - \frac{8y^3}{3} + y\right] \tag{19}$$

where $\alpha = C_S Le + aC_T$, $\Psi_O = 15Ra_{TO}(C_T + \varphi C_S)/8$ and $Ra_{TO} = Ra_T/720$.

Substituting Eqs. (17), (18) and (19) into Eqs. (15) and (16) and integrating yields:

$$C_T = \frac{1}{1+128\Psi_O^2/315}$$

$$C_S = \frac{(1-a)}{1+128Le^2\Psi_O^2/315} + a\frac{(1-128Le\Psi_O^2/315)}{(1+128Le^2\Psi_O^2/315)(1+128\Psi_O^2/315)} \tag{20}$$

Substituting the above values of C_T and C_S into the expression for Ψ_O, the following fifth order polynomial is obtained:

$$\Psi_O\left[Le^4\Psi_O^4 - 2b^2Le^2d_1\Psi_O^2 + 4b^4Le^4\right] - \frac{15}{4}b^2\left[d_2\Psi_O^2 + d_3 2b^2\right] = 0 \tag{21}$$

where $d_1 = -1 - Le^2$, $d_2 = Ra_{To}(Le^4 + \varphi\, Le^2(1-a-a\,Le))$, $d_3 = Le^2 Ra_{T_O}(1+\varphi)$ and $b^2 = 315/256$.

For a given set of the governing parameters, Ra_T, φ, Le and a, the above expression can be solved numerically for Ψ_O and C_T and C_S are evaluated from Eqs. (15) and (16).

It is noted that the above analytical solution is valid independently of the values of the Lewis and Prandtl numbers (provided that this latter, as discussed before, is of order one or greater).Thus, the present model is general and covers the range of binary gas mixtures to that of binary fluid mixtures.

The effect of the thermal Rayleigh number Ra_T on the strength of convection Ψ_O is illustrated in Fig. 2 for the particular case $Le = 5$, $\varphi = 2$ and $a = 1$, i.e. for Soret induced convection. The analytical solution, displayed by a solid line, is seen to be in excellent agreement with the numerical solution of the full governing equations, depicted by black dots. As expected, the results indicate that the convective flow increases monotonously with Ra_T. For large Rayleigh numbers ($Ra_T \to \infty$) the boundary layer regime is eventually reached. For this situation it is readily found from Eq. (21) that:

$$\Psi_O^* = \frac{\Psi_O}{\{1+(\varphi/Le^2)[1-a(1+Le)]\}^{1/3}} = 0.19Ra_T^{1/3} \tag{22}$$

such that the normalized strength of convection Ψ_O^* is independent of both Le and a. This result is presented in Fig. 3 and it is seen that the numerical results obtained for various values

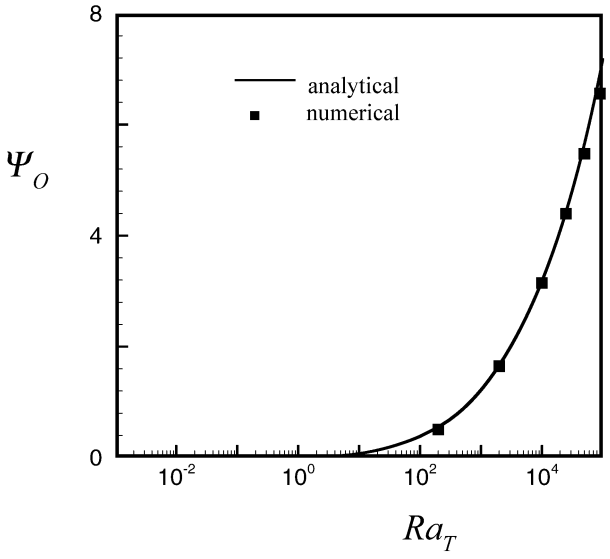

Fig. 2. Effect of Ra_T on Ψ_O for $Le = 5$, $\varphi = 2$ and $a = 1$.

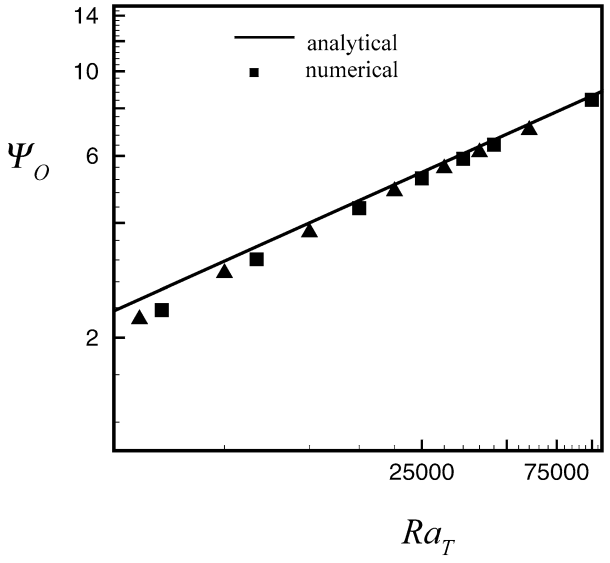

Fig. 3. The boundary layer regime: ▲ $Le = 5$, $\varphi = 1$ and $a = 0$; ■ $Le = 2$, $\varphi = 0$ and $a = 1$.

of Le and a (depicted by symbols) are in agreement with the boundary layer regime (represented by a solid line), Eq. (22), provided that Ra_T is made large enough.

The effect of the buoyancy ratio φ on the intensity of convection Ψ_O is exemplified in Fig. 4 for the case $Ra_T = 2000$, $Le = 2$ and $a = 0$. Excellent agreement is observed between the analytical and the numerical results. The buoyancy ratio φ is varied in the range -5 to 5. This covers the spectrum from opposed but solutal-dominated flow ($\varphi = -5$), to purely thermal-dominated flow ($\varphi = 0$), to aided solutal-dominated flow ($\varphi = 5$). In the absence of solute concentration effects, i.e. when $\varphi = 0$, the flow is induced by the imposed temperature gradients. The resulting flow pattern is a counterclockwise unicellular circulation for which the value of Ψ_O is positive. Increasing the buoyancy ratio from 0 to 5, the flow becomes dominated more-and-more by the mass species buoyant forces.

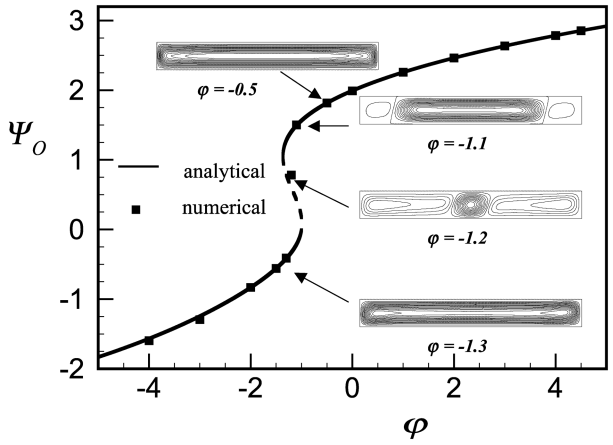

Fig. 4. Effect of φ on Ψ_O for $Ra_T = 2000$, $Le = 2$ and $a = 0$.

On the other hand when φ is below zero, the thermal and solutal forces act now in opposing directions. For $\varphi = -5$ the flow is almost dominated by the mass species. However, since φ is negative, the flow circulation is now clockwise and Ψ_O is negative. Upon increasing the value of φ this situation is maintained up to the particular case $\varphi = -1$ for which the buoyancy forces induced by thermal and solutal effects are opposing each other and of equal intensity. In the range $-1 \leqslant \varphi \leqslant 0$, the thermal buoyancy forces are clearly dominating the flow such that Ψ_O becomes positive. According to the analytical model, it is observed that in the range $-1.39 \leqslant \varphi \leqslant -1$ three solutions, one clockwise circulation and two counterclockwise circulations, are possible. Numerically, transition between the counterclockwise circulation ($\varphi = -0.5$) and clockwise circulation ($\varphi = -1.3$) is illustrated in Fig. 4. Thus for $\varphi = -1.1$ it is observed that the flow pattern consists in a strong counterclockwise cell in the center of the cavity and two weak clockwise cells located in the vicinity of the end regions of the enclosure. As the value of φ is decreased to -1.2 the numerical results indicate that the central counterclockwise is considerably reduced. Thus, for $\varphi = -1.3$, the flow is then unicellular.

5. Particular case ($\varphi = -1$)

This section deals with the particular case where the buoyancy forces induced by the thermal and solutal effects are opposing each other and of equal intensity, $\varphi = -1$. For this situation the rest state is a possible solution provided that the Rayleigh number is below a critical value. In the following subsection this critical Rayleigh number will be predicted on the basis of the linear stability analysis. Then, the parallel flow theory, described in Section 4, will be used to predict the resulting convective flow occurring above the critical Rayleigh number. Finally, the stability of this convective flow will be investigated using the linear stability theory to predict the onset of Hopf bifurcation.

(i) *Stability of the rest state.* For the special case $\varphi = -1$ the purely diffusive state $\Psi_B = 0$, $T_B = S_B = x$ is a solution of the governing set of Eqs. (7)–(9). The stability to small perturbations from the quiescent state of the physical situation described by Eqs. (7)–(9) is examined now. In order to do so, it is convenient to rewrite the governing equations using $\widetilde{\Psi} = \Psi - \Psi_B$, $\widetilde{\Theta} = T - T_B$ and $\widetilde{\Phi} = S - S_B$. As usual, the perturbed solution is assumed to have the following functional form:

$$\widetilde{\Psi}(t,x,y) = F(y)e^{pt+iqx}$$
$$\widetilde{\Theta}(t,x,y) = G(y)e^{pt+iqx}$$
$$\widetilde{\Phi}(t,x,y) = H(y)e^{pt+iqx} \tag{23}$$

where, q is the real vertical wavenumber, $p = p_i + ip_r$ is the complex amplification rate of the perturbation, F, G and H are complex functions satisfying the boundary conditions, given by Eqs. (10) and (11). Inserting the global flow into the governing equations (7)–(9) and linearizing about the basic flow state yields the following set of equations:

$$Pr\left(D^2-k^2\right)^2 F - iqD\psi_B\left(D^2-k^2\right)F + iqD^3\psi_B F - iqRa_T(G-H) = p\left(D^2-k^2\right)\widetilde{\Psi} \tag{24}$$

$$\left(D^2-k^2\right)G - iqD\Psi_B G - C_T DF + iqDT_B F = pG \tag{25}$$

$$\frac{1}{Le}\left(D^2-k^2\right)(H-aG) - iqD\Psi_B H - C_S D\Psi_B + iqDS_B F = pH \tag{26}$$

The corresponding boundary conditions are:

$$y = \pm 1/2, \qquad F = 0; \qquad DG = DH = 0 \tag{27}$$

where $D = \mathrm{d}/\mathrm{d}y$.

The set of Eqs. (24)–(26) is solved using a finite difference scheme. The system is discretized using a fourth order scheme in the domain between $y = -1/2$ and $1/2$, and written in the form $(L_{ij}(q)\vec{Y}_j = pM_{ij}(q)\vec{Y}_j)$. Using a standard subroutine for eigenvalue problems such as EIGENC of IMSL, the eigenvalues are evaluated as a function of the control parameters, Ra_T, Le, Pr, a and the wave number q. For given values of Ra_T, Le, Pr and a, one can determine the value of Ra_T for which the fastest growth rate (maximal value of p_r) cancels out. This gives a functional $Ra_T = Ra_T(q, p_i)$. The minimum in the marginal stability curve $R_T(q)$ determines the critical state parameters (q_C, p_{iC}, Ra_{TC}). The numerical procedure was found to converge for a discretization number n superior at 100.

In this way it can be demonstrated that the supercritical Rayleigh number for the onset of convection is given by (see for instance [17])

$$Ra_{TC}^{\sup} = \frac{R}{[(Le+a)-1]} \tag{28}$$

where R is a constant which depends upon the aspect ratio of the layer. Thus for $A \to \infty$ it is found that $R = 6505$. For the case of double diffusive convection in a rectangular cavity subject to opposing horizontal fluxes of heat and concentration of equal intensity (double diffusive convection, $a = 0$) it was found by Mamou [18] that $Ra_{TC}^{\sup} = 6510/(Le-1)$. Thus the constant R has about the same value that obtained in the present study. However, the dependence of $Ra_{TC}^{\sup}$ on Le is observed to be different since the present analysis has been extended to

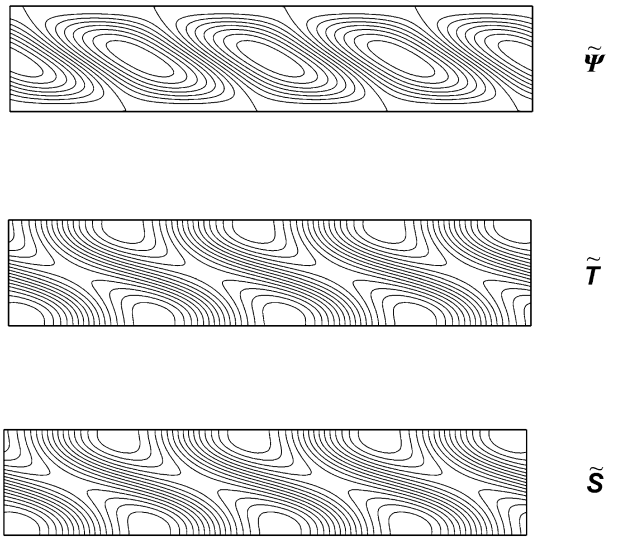

Fig. 5. Numerical results for the onset of convection as predicted by the linear stability analysis streamlines; isotherms and isoconcentrations patterns for $R = 6505$, $Le = 10$ and $a = 1$.

predict both double diffusive convection and Soret induced convection.

Fig. 5(a) presents the streamlines at the onset of supercritical convection for $Le = 10$ and $a = 1$. The results indicate the existence of a flow structure of tilted counter-rotating roll cells in the horizontal direction with a wave number $q_C = 2.53$. The corresponding temperature perturbation $\widetilde{\Theta}$ and concentration perturbation $\widetilde{\Phi}$ are depicted in Figs. 5(b) and 5(c), respectively.

(ii) *Convective flow.* For the particular case, $\varphi = -1$, it can be easily demonstrated that the resulting solution is given by Eqs. (17)–(20), were the value of Ψ_O can be evaluated from the following expression:

$$\Psi_O\left[\Psi_O^4 c^2 Le^2 + \Psi_O^2 c\left(1 + Le^2\right) - 2\Psi_O\sqrt{c}Ra_{T_O}\left(Le^2 + (a-1) + a\,Le\right) + 1\right] = 0 \qquad (29)$$

where $c = 315/128$ and $Ra_{T_O} = Ra_T\sqrt{c}/768$.

It is seen from the present theory that the onset of motion, occurs at a subcritical Rayleigh number Ra_{TC}^{sub} given by

$$Ra_{TC}^{\text{sub}} = \frac{768(\Psi_C^3 Le^2 c^2 + \Psi_C c(Le^2+1) + 1/\Psi_C)}{2\sqrt{c}(Le^2 - 1 + a(Le+1))} \qquad (30)$$

where

$$\Psi_C = \pm\left[\sqrt{\left(Le^2+1\right)^2 + 12Le^2} - \left(Le^2+1\right)\right]^{1/2}/\sqrt{6c}\,Le \qquad (31)$$

In Fig. 6 the stream function amplitude Ψ_O is plotted as a function of Ra_T for $Le = 10$ and $a = 0$. For this situation, according to Eqs. (28) and (30), $Ra_{TC}^{\text{sub}} = 123$ and $Ra_{TC}^{\text{sup}} = 723$. For convenience, these values are indicated on the graph by vertical dotted lines. Upon starting the numerical code with a conductive state or a finite-amplitude state convection as initial conditions, when increasing or decreasing Ra_T, the resulting solution follows the hysteresis loop indicated by arrows. The analytical solution, depicted by the solid and dashed lines, indicates the possible existence of two convective modes for a given

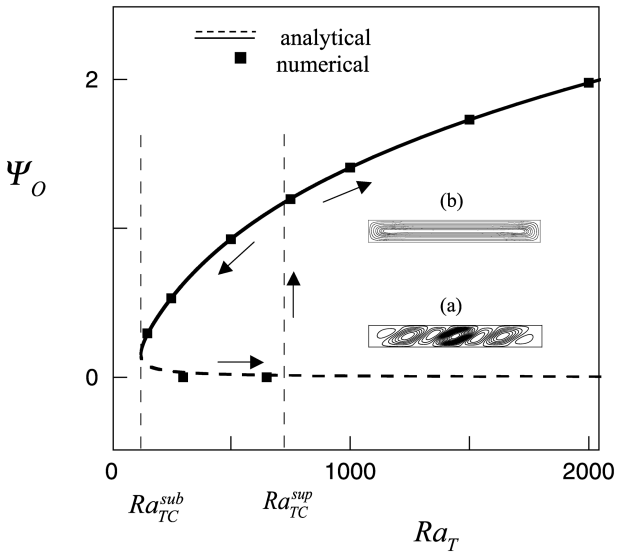

Fig. 6. Bifurcation diagram for $Le = 10$, $\varphi = -1$ and $a = 0$.

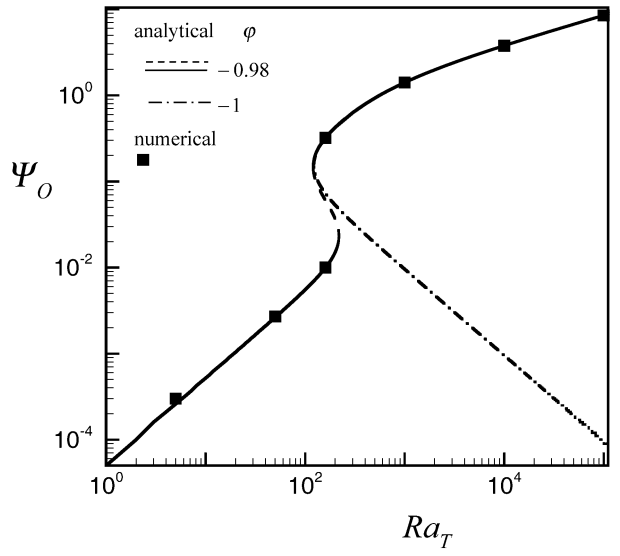

Fig. 7. Bifurcation diagram for $Le = 10$, $a = 0$, $\varphi = -1$ and $\varphi = -0.98$.

value of Ra_T. The solution corresponding to the higher convective mode (solid line), was found numerically to be stable. On the other hand it has not been possible to obtain numerical results for the lower (dashed line) unstable branch.

The flow pattern (a), presented in Fig. 6, is the result of the numerical solution obtained for the case $Ra_T = 750$, at time $t = 8$, for which the solution is not permanent. The resulting flow configuration, consisting in inclined cells, is similar to the prediction of the linear stability analysis (Ref. [18]). However, for $t \geqslant 17.5$, the numerical procedure becomes permanent and the resulting flow pattern (b) indicates the existence of a unicellular convection flow, in agreement with the analytical prediction.

Fig. 7 presents the bifurcation diagram obtained by the present theory and the numerical solution for the case $Le = 10$, $a = 0$, $\varphi = -0.98$ and -1, respectively. For low values of Ra_T it is observed that for the case $\varphi = -0.98$ convection is

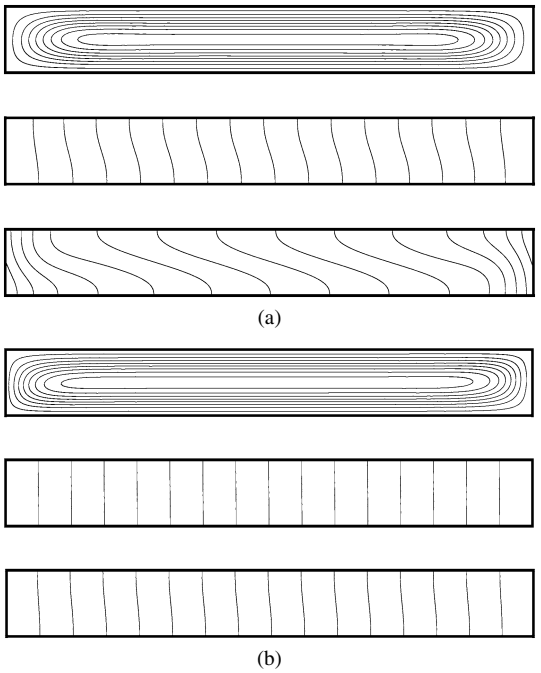

Fig. 8. Contour lines of stream function (top), temperature (middle) and concentration (bottom) for $Ra_T = 160$, $Le = 10$, $\varphi = -0.98$ and $a = 0$.

weak and can be seen as a degeneracy of the conductive solution obtained for $\varphi = -1$. This type of flow is maintained up to a critical Rayleigh number ($Ra_T \approx 120$) where a first saddle-node bifurcation occurs. This unstable branch (shown as a dotted line) is connected to another saddle-node bifurcation occurring at a critical Rayleigh number ($Ra_T \approx 219$). Then, upon increasing the Rayleigh number the results obtained for $\varphi = -0.98$ and -1 are approximately the same. In the region between $120 \leqslant Ra_T \leqslant 219$ three solutions are possible for a given Rayleigh number, one of which (the dotted line branch) is unstable.

The existence of multiple solutions in the range $120 \leqslant Ra_T \leqslant 219$ was demonstrated numerically for the case $Ra_T = 160$, $Le = 10$, $\varphi = -0.98$ and $a = 0$. Fig. 8(a) shows the results obtained by using the rest state and uniform temperature and concentration as initial conditions for the numerical code. The resulting flow in the core of the layer is observed to be parallel while the temperature and concentration are linearly stratified in the horizontal direction. Due to the strength of convection ($\Psi_C = 0.32$, where Ψ_C is the value of the stream function at the center of the cavity) the existence of concentration gradient reversal is observed to occur in the core of the cavity. Starting the numerical solution with the convective flow obtained for instance at $Ra_T = 100$ ($< Ra_T = 120$) yields the results depicted in Fig. 8(b). The strength of flow circulation is found to be considerably weaker ($\Psi_C = 0.01$) as indicated by the temperature and concentration fields which are now almost purely diffusive. Fig. 9 shows the velocity profiles corresponding to these two solutions. The excellent agreement between the analytical and the numerical solutions is noticed. The third analytical velocity profile predicted by the analytical solution is unstable and as such could not be verified by the numerical code.

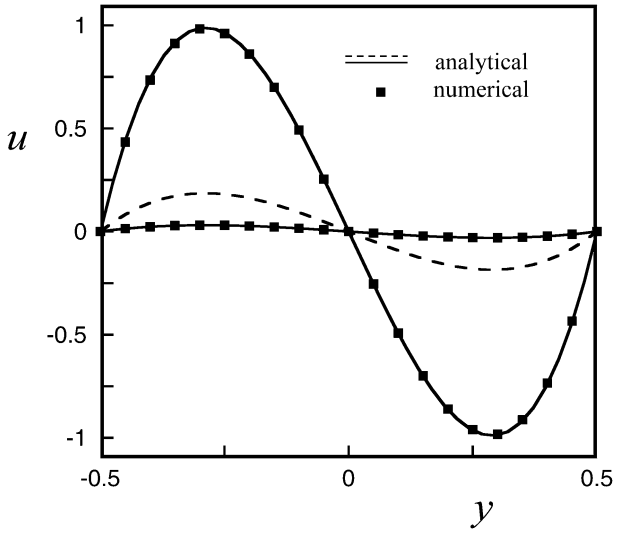

Fig. 9. Multiple solutions for $Ra_T = 160$, $Le = 10$, $\varphi = -0.98$ and $a = 0$.

6. Summary

In this article, the problem of natural convection in a horizontal fluid layer subject to horizontal gradients of temperature and solute has been solved by both analytical and numerical methods. The influence of the thermal Rayleigh number Ra_T, buoyancy ratio φ, Lewis number Le and parameter a (=0, double diffusive convection; and =1 Soret induced convection) on the intensity of convection were predicted and discussed. The summary of the major results is:

(i) An analytical solution, based on the parallel flow approximation, has been derived for the case of a shallow layer $A \gg 1$. Although, the resulting analytical model requires a numerical procedure to solve a transcendental equation, this is by far a much easier task than solving numerically the full set of governing equations. Furthermore, in the boundary layer regime, the present analysis yields a set of closed-form solutions.

(ii) The particular solution $\varphi = -1$, for which the buoyancy forces induced by the thermal and solutal effects are opposing each other and of equal intensity has been considered. For this situation, a steady rest state solution corresponding to a purely diffusive regime is possible. The critical Rayleigh number, $Ra_{TC}^{\sup}$, for the onset of supercritical convection has been predicted numerically, on the basis of the linear stability theory. Also, the subcritical Rayleigh number, Ra_{TC}^{sub}, for the onset of subcritical convection is deducted from the nonlinear parallel flow approximation. In the vicinity of $\varphi = -1$, the existence of multiple solutions, for a given set of the governing parameters is demonstrated both analytically and numerically.

The features of the analytical model were strongly confirmed by numerical simulations of the full governing equations.

Acknowledgement

This work was supported by the Natural Sciences and Engineering Research Council, Canada.

References

[1] O.V. Trevisan, A. Bejan, Combined heat and mass transfer by natural convection in a vertical enclosure, Int. J. Heat Mass Transfer 109 (1987) 104–112.
[2] F. Alavyoon, On natural convection in a vertical porous enclosure due to prescribed fluxes of heat and mass at the vertical boundaries, Int. J. Heat Mass Transfer 36 (1993) 2479–2498.
[3] P. Ranganathan, R. Viskanta, Natural convection in a square cavity due to combined driving forces, Numer. Heat Transfer 14 (1988) 35–39.
[4] K. Han, T. Kuchn, Double diffusive convection in a vertical rectangular enclosure—I experimental study, Int. J. Heat Mass Transfer 34 (1991) 449–459.
[5] J. Lee, M.T. Hyun, W. Kim, Natural convection in confined fluids with combined horizontal temperature and concentration gradients, Int. J. Heat Mass Transfer 31 (1988) 1969–1977.
[6] J. Lee, J.M. Hyun, Double-diffusive convection in a rectangle with opposing horizontal temperature and concentration gradients, Int. J. Heat Mass Transfer 33 (1990) 1619–1632.
[7] W. Shyy, M. Chen, Double-diffusive flow in enclosures, Phys. Fluids A 3 (1991) 2592–2602.
[8] M. Mamou, P. Vasseur, E. Bilgen, Analytical and numerical study of double diffusive convection in a vertical enclosure, Heat Mass Transfer 32 (1996) 115–125.
[9] T.L. Bergman, R. Srinivasan, Numerical simulation of Soret-induced double diffusion in an initially uniform concentration binary fluid, Int. J. Heat Mass Transfer 32 (1989) 679–687.
[10] Ph. Traore, A. Mojtabi, Analyse de l'effet Soret en convection thermosolutale, Entropie 184/185 (1989) 32–37.
[11] R. Krishnan, A numerical study of the instability of double-diffusive convection in a square enclosure with horizontal temperature and concentration gradients, Heat transfer in convective flows, HTD ASME National Heat Transfer Conference, Philadelphia 107 (1989) 357–368.
[12] D. Gobin, R. Bennacer, Double-diffusion convection in a vertical fluid layer : onset of the convection regime, Phys. Fluids 6 (1994) 59–67.
[13] S.R. De Groot, P. Mazur, Non-Equilibrium Thermodynamics, North-Holland, Amsterdam, 1969.
[14] S.V. Patankar, Numerical Heat Transfer and Fluid Flow, Hemisphere, Washington, DC, 1980.
[15] M. Mamou, P. Vasseur, Hasnaoui, On numerical stability analysis of double-diffusive convection in confined enclosures, J. Fluid Mech. 433 (2001) 209–250.
[16] M. Mamou, P. Vasseur, Thermosolutal bifurcation phenomena in porous enclosures subject to vertical temperature and concentration gradients, J. Fluid Mech. 395 (1999) 61–87.
[17] A. Bahloul, N. Boutana, P. Vasseur, Double-diffusive and Soret induced convection in a shallow horizontal porous layer, J. Fluid Mech. 491 (2003) 325–352.
[18] M. Mamou, Convection thermosolutale dans des milieux poreux et fluides confinés, PhD thesis, Université de Montréal, 1998.